JOURNAL OF MATERIALS SCIENCE **38** (2003) 4817–4830

Microstructural characterization of porous manganese thin films for electrochemical supercapacitor applications

B. DJURFORS
Department of Chemical and Materials Engineering, University of Alberta, Edmonton, Alberta T6G 2G6, Canada
E-mail: djurfors@ualberta.ca

J. N. BROUGHTON, M. J. BRETT
Department of Electrical and Computer Engineering, University of Alberta, Edmonton, Alberta T6G 2G6, Canada

D. G. IVEY
Department of Chemical and Materials Engineering, University of Alberta, Edmonton, Alberta T6G 2G6, Canada

An in-depth microstructural characterization was performed on manganese oxide materials that have been produced for electrochemical supercapacitor applications using a novel physical vapor deposition process. Manganese was e-beam evaporated and deposits as a combination of the cubic forms of Mn and MnO with a porous zigzag structure. The electrochemically oxidized sample that is used as the supercapacitor base material is tetragonal Mn_3O_4. An apparent active layer with increased sodium levels was imaged by STEM, lending some credence to the argument that the pseudocapacitance effect is based entirely on a surface layer of adsorbed sodium. Upon furnace annealing the zigzag structure near the free surface is destroyed and replaced with a columnar oxide layer of cubic MnO and tetragonal Mn_3O_4. This capping effect ultimately reduces the usable surface area and is thought to account for the reduction in capacitance seen on annealing.

1. Introduction

Electrochemical supercapacitors are capacitors that make use of electrochemical phenomena in order to store charge. As charge storage devices, they are primarily used for applications that require a high power output, and a high cycle capacity. They are often used in conjunction with other energy storage devices, such as batteries, in an attempt to improve the overall performance of the system by supplementing the continuous power output of the battery with periodic bursts of high power provided by the electrochemical supercapacitor. Their advantage over traditional capacitors is a significantly improved capacitance per unit mass [1, 2].

Electrochemical supercapacitors can be of two types: double layer capacitors and redox supercapacitors. The former type is comparable to a traditional capacitor as it employs the non-Faradic charge separation that occurs naturally across a double layer in an electrochemical cell in order to store charge. Activated carbon materials are predominantly used for this purpose because of their relatively low cost and high surface area (up to 2500 m^2/g) [2]. The redox supercapacitor makes use of a reversible redox reaction in order to store charge. The behavior is typically termed "pseudocapacitance" and resembles a re-chargeable battery more than a traditional capacitor [1]. In addition, the charge storage mechanism is Faradic as charge passage across the double layer is integral to the workings of the device. Traditionally, ruthenium oxide has found success as a pseudocapacitor exhibiting specific capacitance values of up to 750 F/g. However, cost is prohibitive to large-scale commercial production [2].

Manganese and its oxides have enjoyed some interest as replacement materials for the more costly ruthenium oxides in electrochemical supercapacitor applications because of their relatively low cost and toxicity [3]. Typically, MnO_2 films have been created by chemical reactions and often result in an amorphous hydrated MnO_2 product or a weakly crystalline hydrated MnO_2 product [3–8]. Recently a new technique for producing manganese supercapacitor materials was developed by Broughton and Brett making use of physical vapor deposition and an oblique vapor incidence angle in order to produce a porous metallic structure instead of employing the more common wet chemistry method [9]. Using a glancing angle deposition (GLAD) process, manganese films were deposited with a chevron

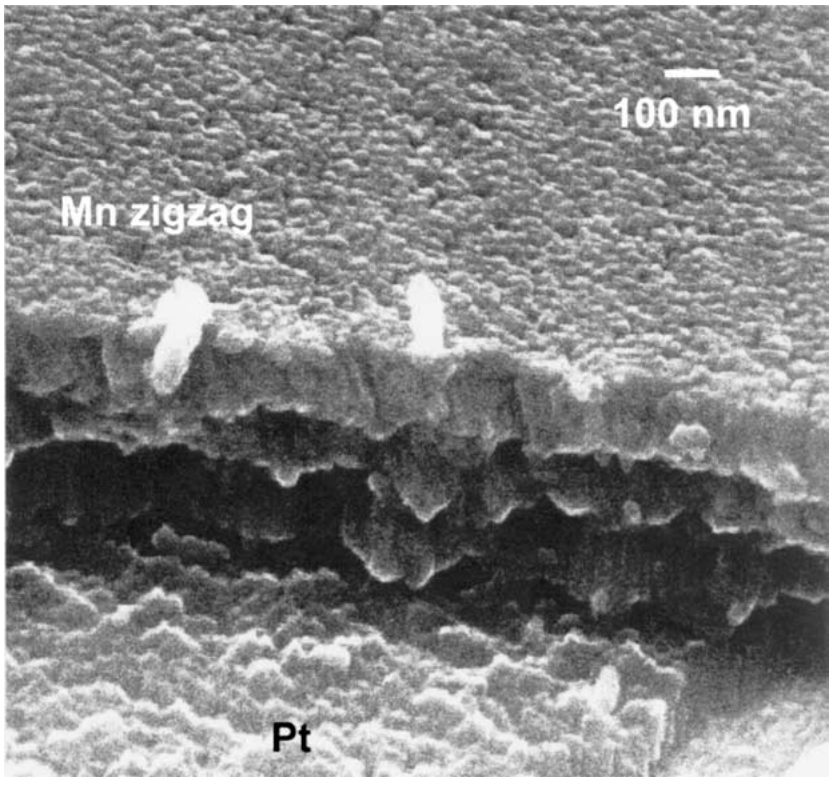

(a)

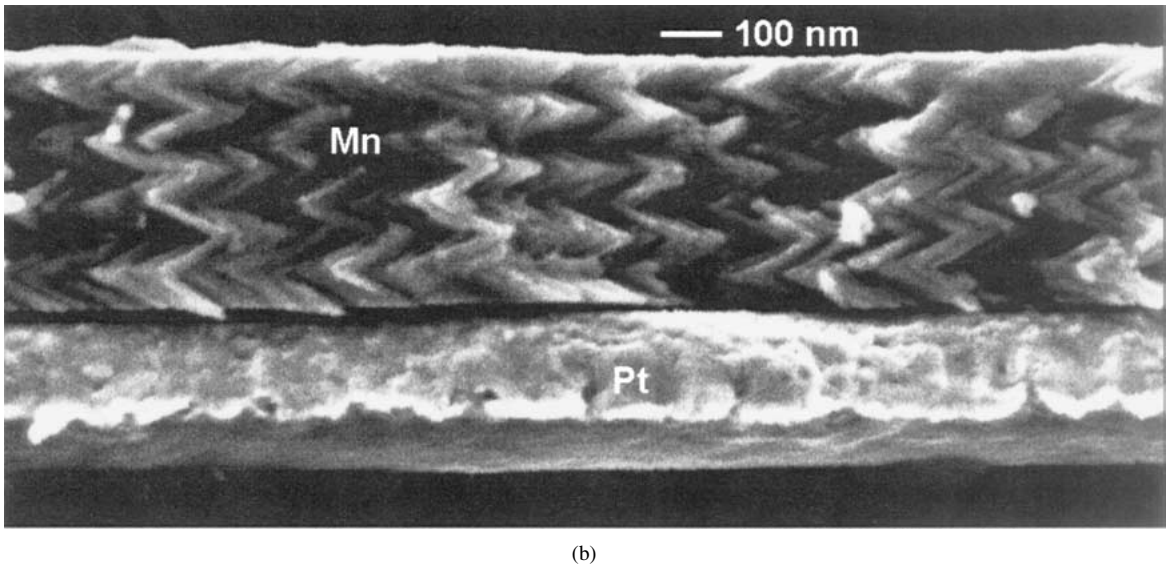

(b)

Figure 1 FE-SEM secondary electron (SE) images of the as-deposited manganese film revealing the surface texture (a) and the cross-sectional morphological texture (b).

structure of varying porosity, all of which exhibit supercapacitive behavior. Although the specific capacitance realized by these films, 225 ± 25 F/g, has not yet achieved the levels of Chin *et al*. [10] (720 F/g), the procedure has shown promise. Initial results revealed that above a 70° vapor incidence angle, the capacitance value for these films remains approximately constant. Some research has indicated that limited furnace annealing can enhance the specific capacitance of the film [10], however, annealing of the chevron films was found to prevent the film from becoming supercapacitive [9].

What is lacking in the original analysis of this method is an understanding of the phases involved and produced during the deposition, thermal annealing, and the electrochemical oxidation of the supercapacitor. A clear understanding of the phases and phase evolution will help in any work to modify and improve the supercapacitive behavior. The purpose of this research is to study the manganese electrochemical supercapacitor films in their as-deposited, electrochemically oxidized, and furnace annealed states in order to conclusively determine which phases are present during each stage and suggest improvements in processing that may help this technique achieve the high capacitance values of Chin *et al*. [10]. X-ray diffraction, electron diffraction, transmission electron microscopy and scanning electron microscopy, are used to characterize the materials.

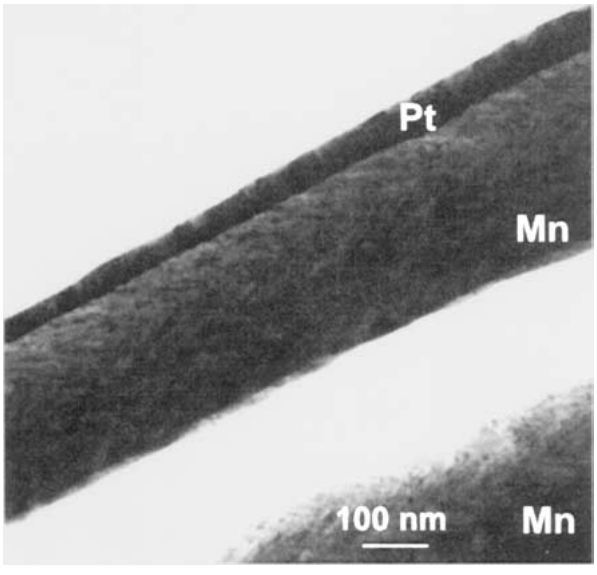

(a)

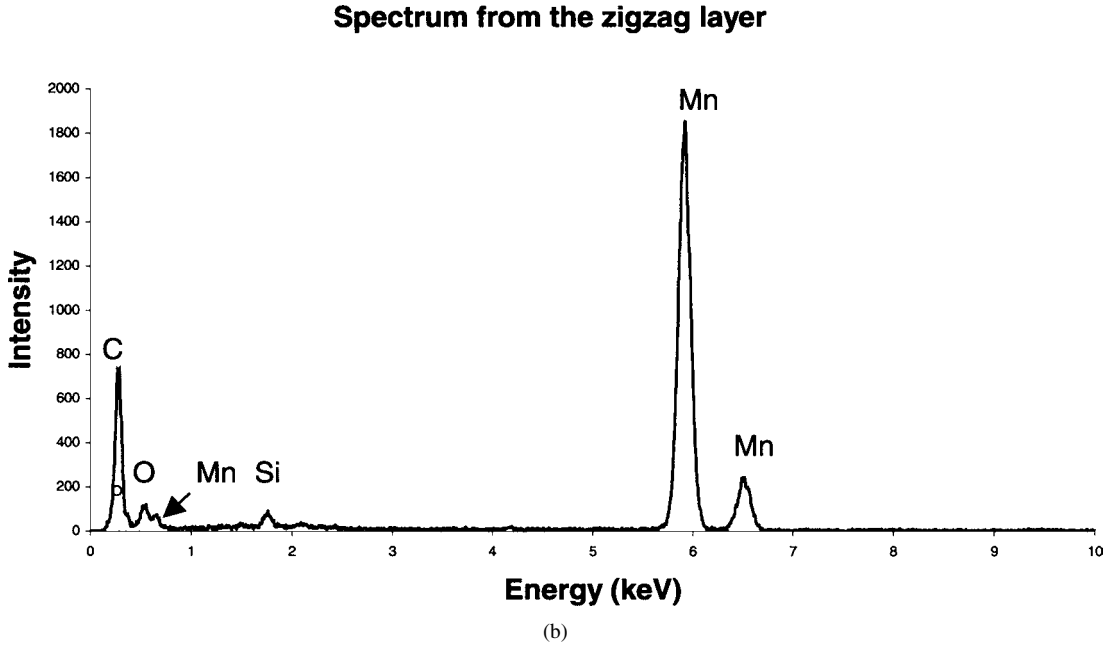

(b)

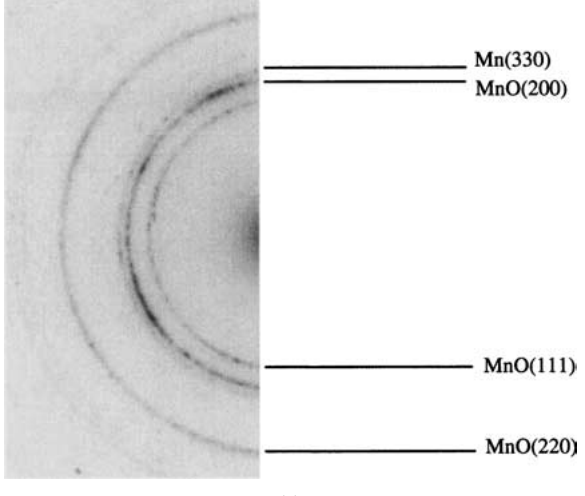

(c)

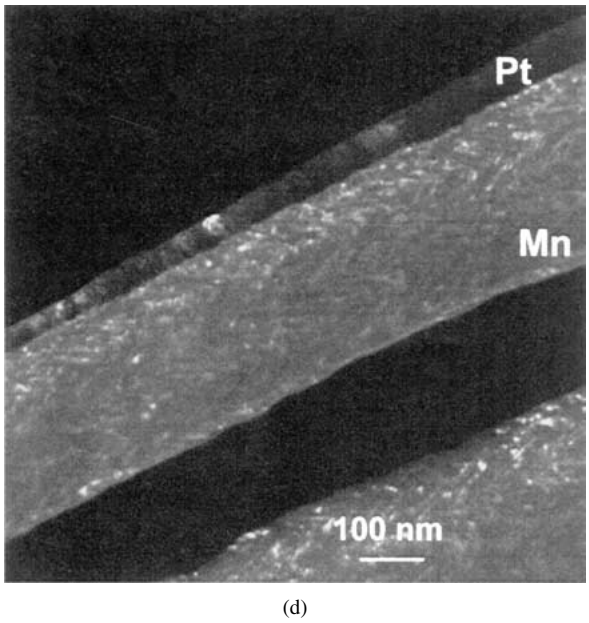

(d)

Figure 2 (a) Cross-section TEM BF image of the as-deposited film. (b) EDX spectrum from the zigzag layer shown in Fig. 2a. (c) Indexed SAD pattern from the deposited zigzag layer. (d) TEM DF image of deposited layer from part of the 111, 200 reflections for the MnO and part of the 330 reflection for the Mn.

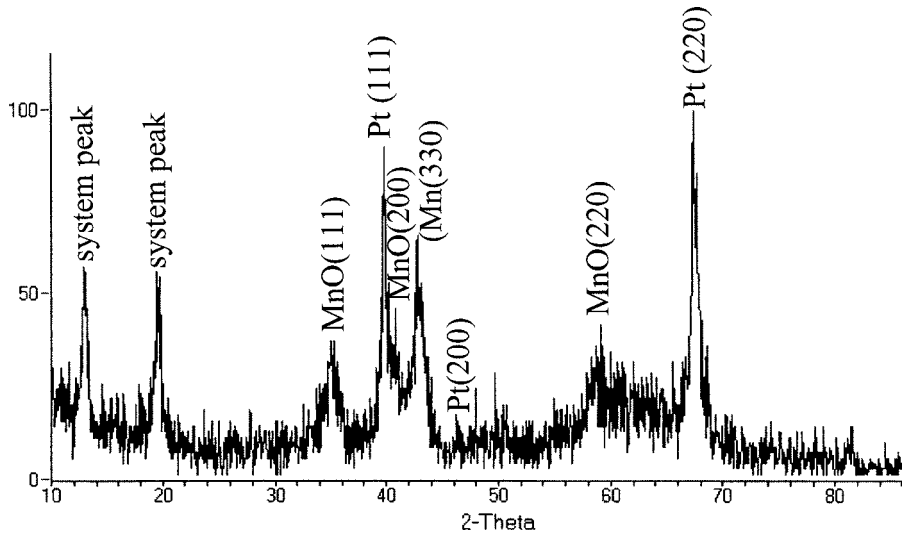

Figure 3 XRD pattern from as-deposited film showing Mn and MnO.

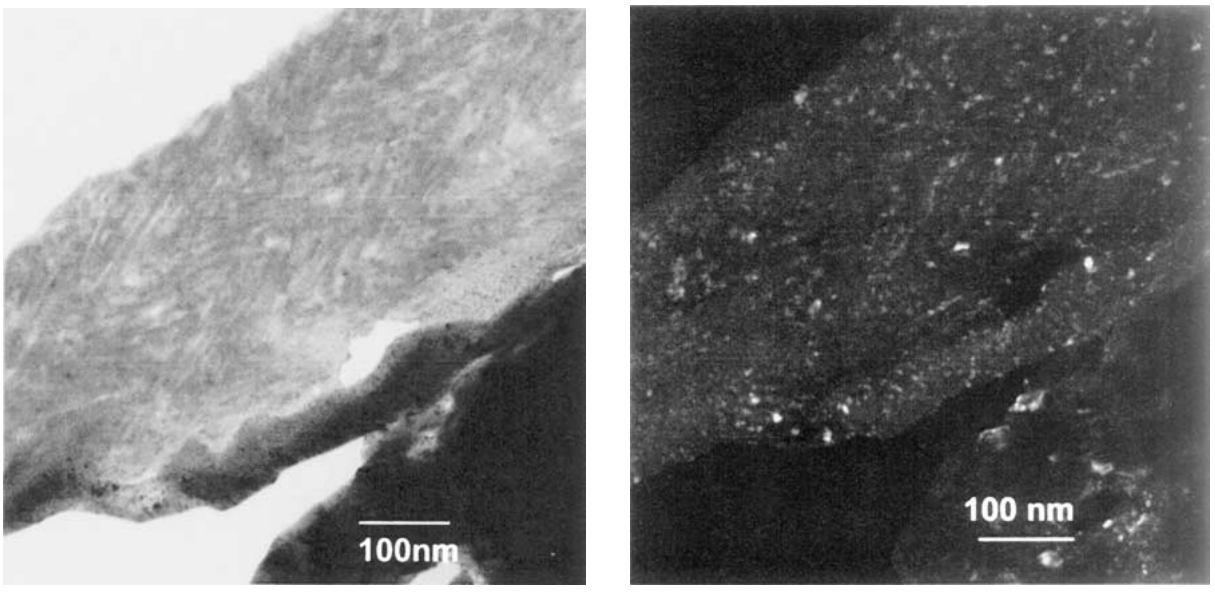

(a) (b)

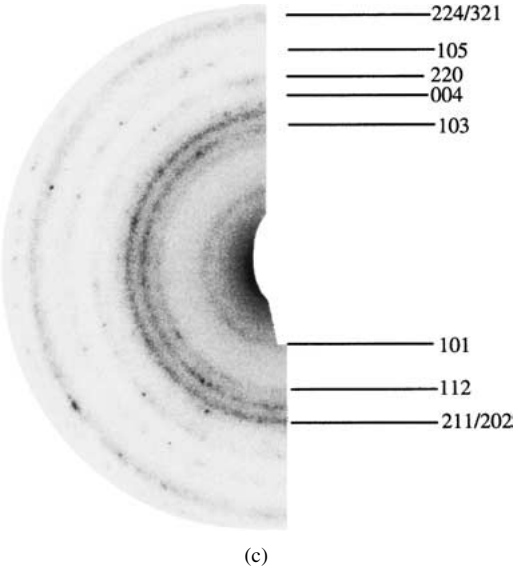

(c)

Figure 4 (a) TEM BF image of the electrochemically oxidized sample in cross-section. (b) DF image of the same sample from part of the (105) reflection. (c) SAD pattern from the area shown in (a) indexed for the tetragonal Mn_3O_4 phase.

2. Experimental procedure

The manganese films were fabricated in a vacuum evaporator, that was fitted with a glancing angle deposition (GLAD) system as described previously, using a pure manganese source [9]. The manganese films were deposited on Si substrates coated with a layer of SiN to provide a dielectric, followed by a Ti/Pt metallization layer for adhesion. The films were made with a chevron texture utilizing an incidence flux angle of 77°, with a base pressure of approximately 5×10^{-7} torr. The furnace-annealed samples were annealed in a standard furnace with an air atmosphere at 300°C for a range of times: 30, 60, 120, and 1920 min. Finally, electrochemically oxidized samples were produced by immersion in a 0.1 M Na_2SO_4 electrolyte using a Pine Instruments AFCBP1 potentiostat, with an Ag/AgCl reference electrode, a Pt wire as the counter electrode, and a sweep rate of 50 mV/s. The sample was electrochemically oxidized by slowly increasing the voltage during the initial charging cycle. Once the sample was fully oxidized, charging and discharging occurred at a much faster rate. More complete details of the electrochemical characterization of these films can be found in the original reference [9].

The samples were imaged first in a JEOL field emission scanning electron microscope (FE-SEM) at 5 kV without any conductive coating. Some charging was evident producing noise in the images. Higher resolution imaging was done primarily in a JEOL 2010 transmission electron microscope (TEM) with a Noran ultra-thin window (UTW) X-ray detector for compositional analysis. Both plan view and cross-section samples were imaged at 200 kV. Crystal structure analysis was done using electron diffraction patterns. Higher spatial resolution analysis was done on select samples using a Technai F20 field emission gun (FEG) TEM/STEM. Images were obtained in STEM mode using the annular dark field detector, which provided better contrast for thicker samples.

Cross-section samples were made using the following procedure. Two pieces of equal size were first cleaved from the sample. The two pieces, with deposit surfaces facing each other, were glued together. Scrap Si pieces were used as supports on either side of the glued samples to build a raft structure. The raft was then ground to a thickness of 200 μm, after which a 3 mm disk was machined from the raft with the sample interface centered in the disk. The disk was dimpled on both sides until optical transparency was reached ($\sim$30 μm) at the centre. The sample was sputtered from both sides, with a current of 0.5 mA per gun at 5 kV and an incidence angle of 85°, until perforation. At this time, the incident angle was increased to 87° and the current and gun energy lowered to 0.3 mA per gun and 4 kV respectively, to reduce ion damage. Sputtering was continued for 40 min, or until a smooth edge at the hole was formed. All samples were cooled with liquid nitrogen prior to and during sputtering, to reduce preferential sputtering effects. Plan view samples were made by dimpling from the back side of the material to approximately 10 μm in thickness. Then, the sample was sputtered from the substrate side only using the same conditions as above.

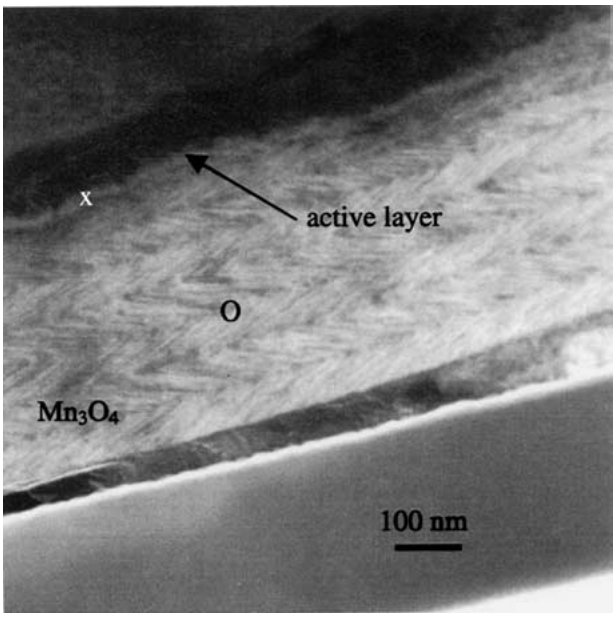

(a)

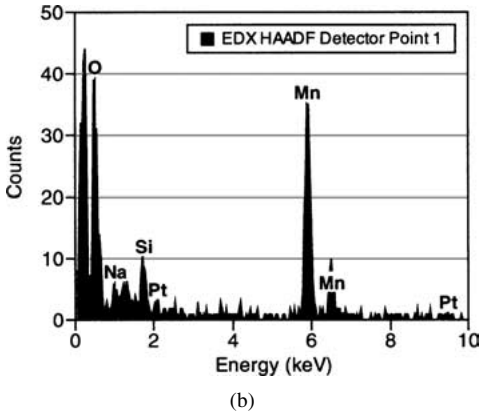

(b)

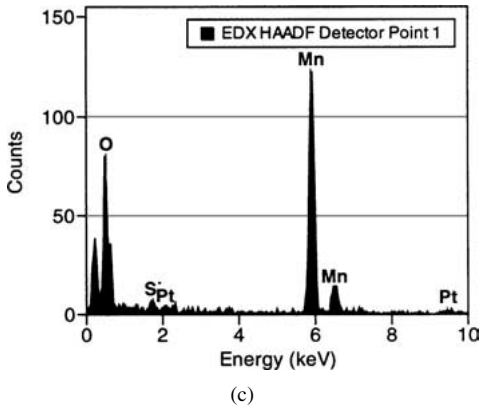

(c)

Figure 5 (a) STEM annular DF image of the electrochemically oxidized sample, (b) EDX spectrum taken from the thin layer region marked with an X and (c) EDX spectrum taken from the bulk sample region marked with an O.

X-ray diffraction (XRD) analysis was done using a Rigaku Rotaflex rotating anode diffractometer with a thin film camera attachment. The filament voltage and current were set at 40 kV and 110 mA respectively. Samples were scanned between 10° and 90° at a rate of 2°/min using an X-ray incidence angle of 2° to ensure no substrate was sampled. A blank wafer with just

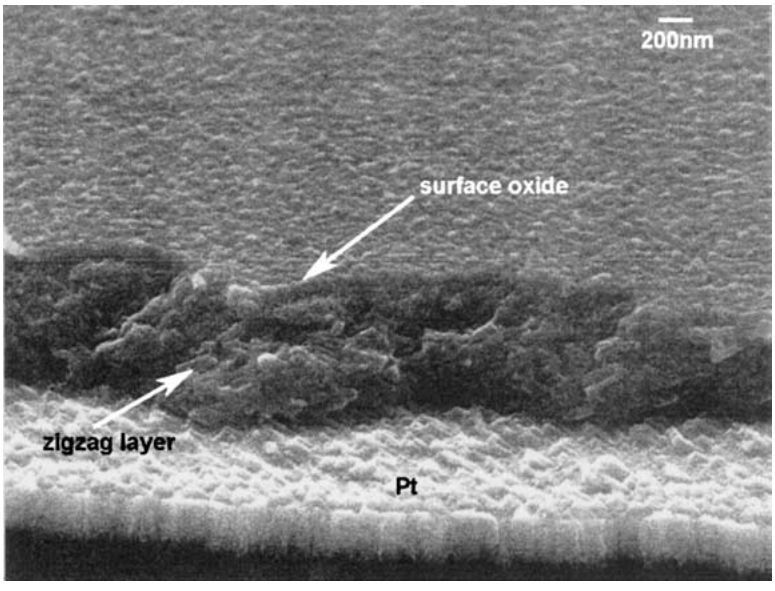

(a)

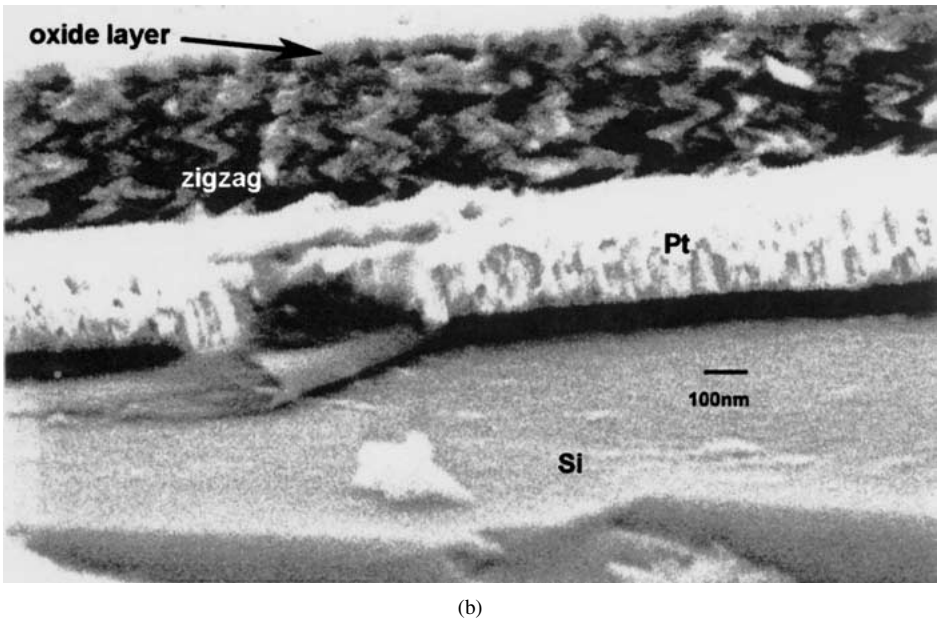

(b)

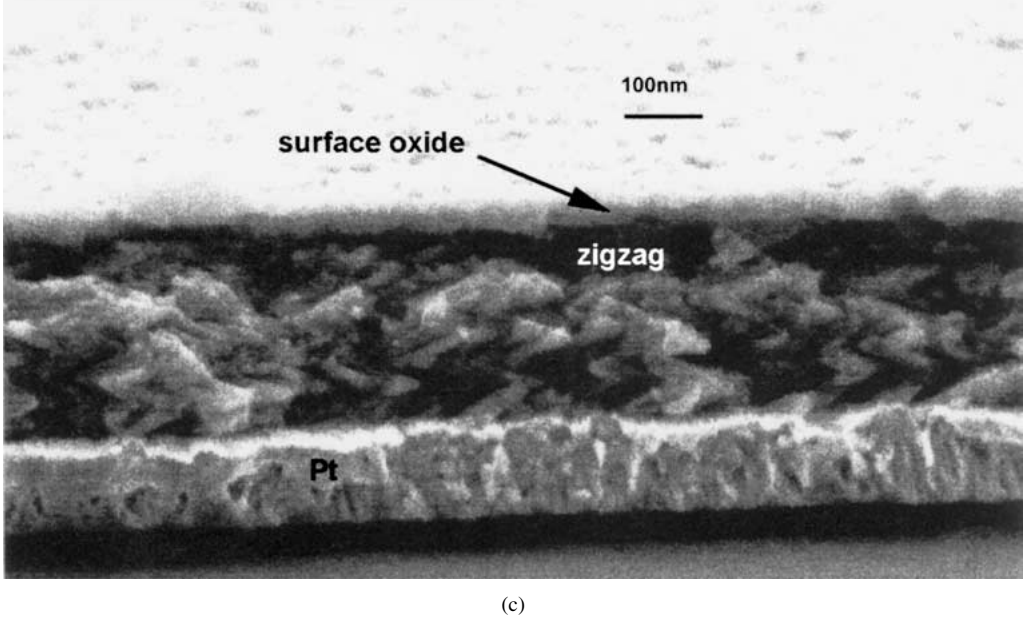

(c)

Figure 6 FE-SEM SE images of the zigzag layer annealed for (a) 30 min, (b) 60 min, (c) 120 min, and (d) 1920 min. (*Continued*)

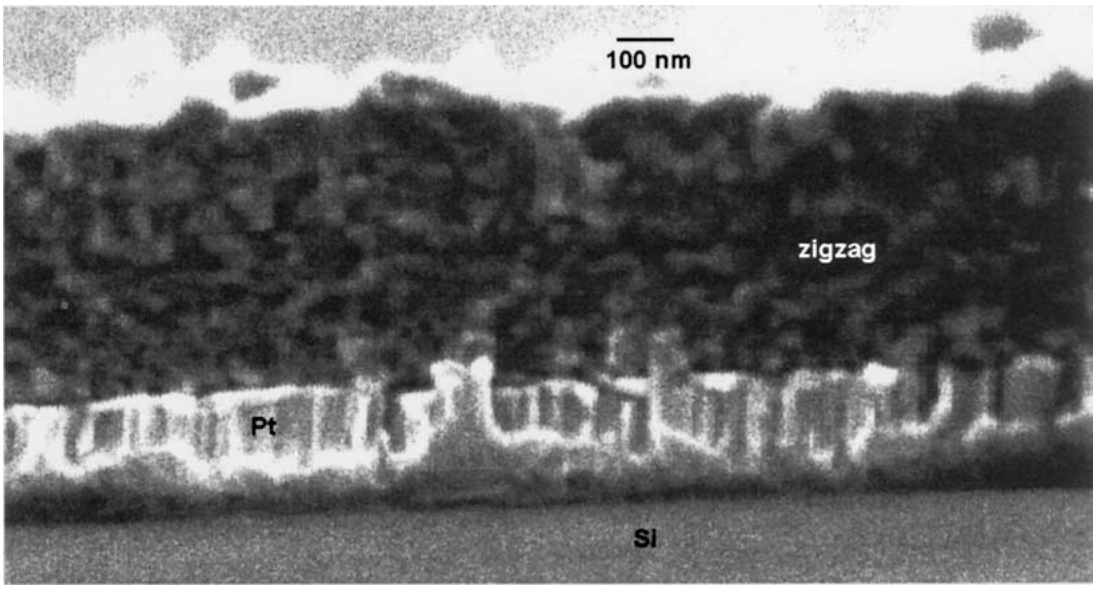

(d)

Figure 6 (*Continued*)

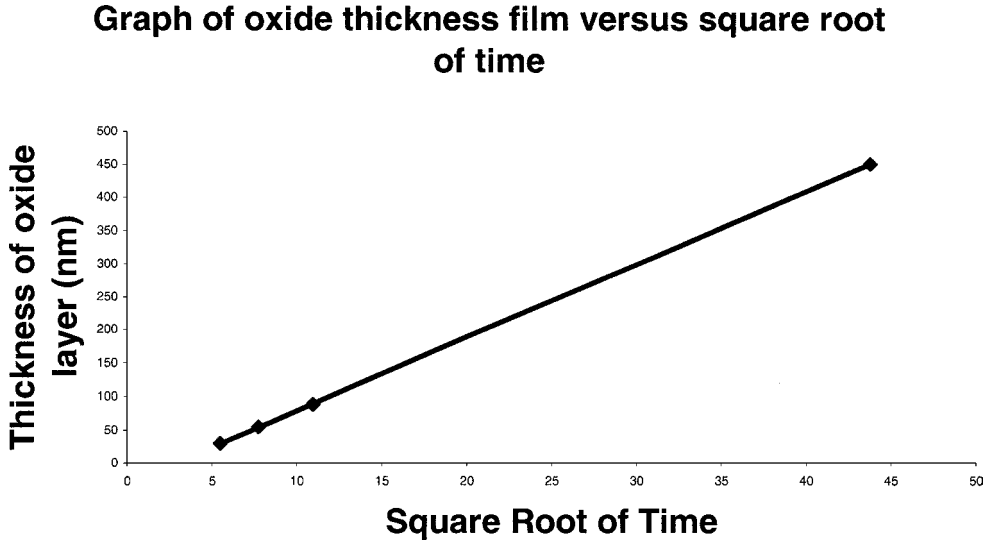

Figure 7 Plot of oxide layer thickness versus annealing time.

the metallization layers, prior to manganese deposition, was run for background signal comparison and elimination.

3. Results/discussion

3.1. As-deposited

Because the sample is initially deposited as a metal film, and later annealed or electrochemically oxidized in solution during the initial charge cycle, it is important to establish an initial state. As a result, the as-deposited film was studied quite extensively in order to determine the starting material. The initial FE-SEM image of the as-deposited structure is shown in Fig. 1. The approximate porosity of the film surface is shown in Fig. 1a, although the zigzag structure is not visible as the image was taken in plane with the zigzags. Fig. 1b does, however, show the typical zig-zag structure of the manganese chevron texture produced at a 77° flux incidence angle.

Fig. 1b also reveals that the zigzags are quite close together, severely limiting the macroporosity of the structure. The dark areas are not porosity, but missing material removed as a result of cleaving during specimen preparation. If in-plane zigzags are observed, there is very little macroporosity between the individual columns.

The internal structure of the film is revealed in TEM cross-sectional images, both bright field and dark field (Fig. 2). The bright field image (Fig. 2a) of the as-deposited film reveals that the film, while exhibiting a chevron structure that is visible in Fig. 1, is still quite dense. In fact, there does not appear to be any macroporosity (between the zigs and zags). Comparison of the image with Fig. 1 shows that the only visible porosity appears to be in the final portion of the film that is deposited, i.e., the small visible space between the individual columns near the surface of the film. This is clearly not the ideal structure for supercapacitive applications, as the reaction surface is

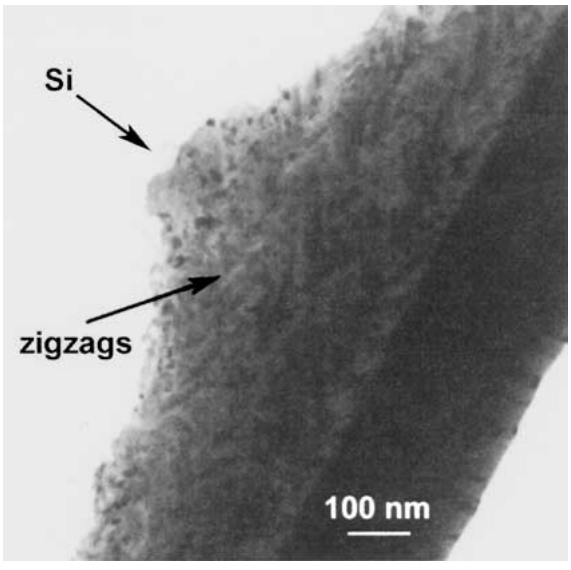

(a)

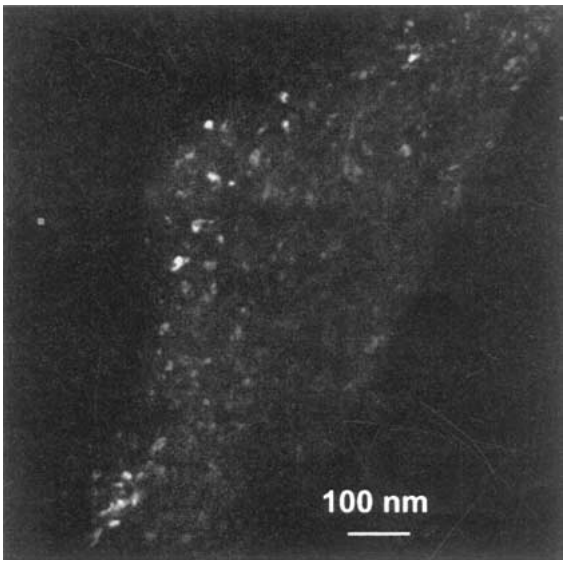

(b)

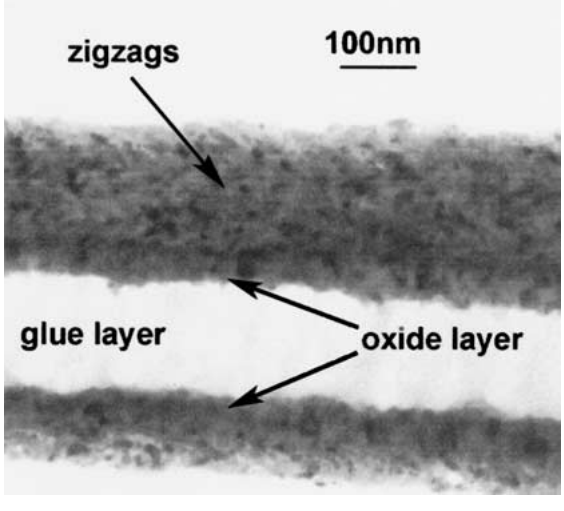

(c)

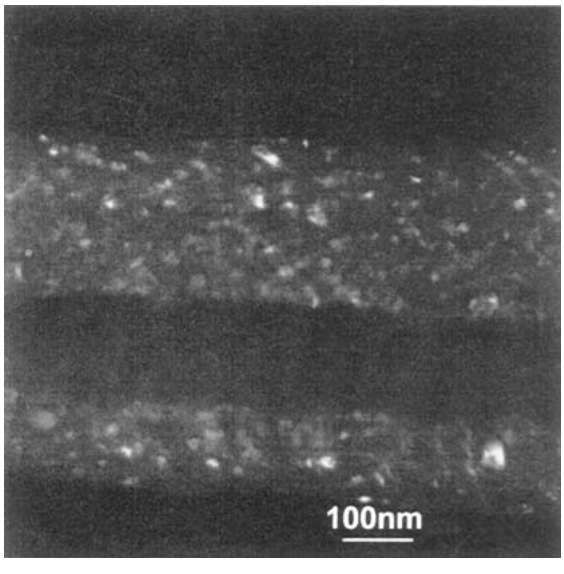

(d)

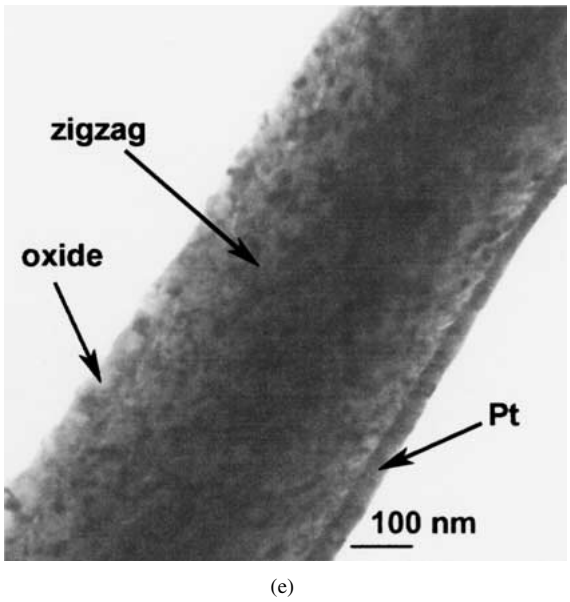

(e)

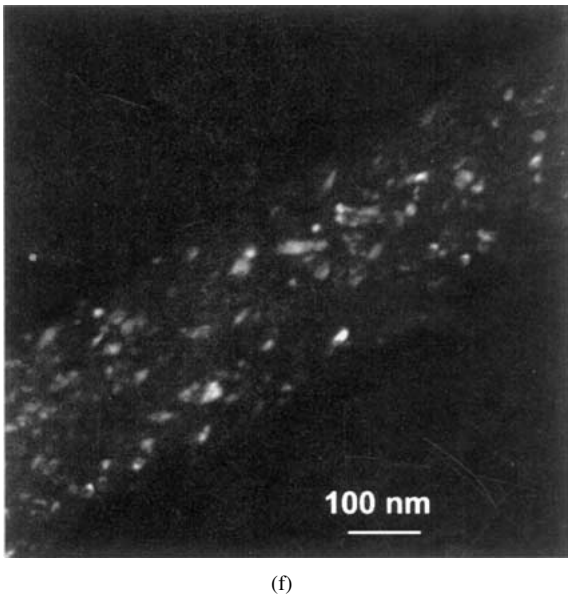

(f)

Figure 8 (a) TEM BF image of a cross-section sample of the layer annealed at 300°C for 30 min. (b) TEM DF image of the annealed zigzag layer in (a) using part of the 111 and 200 reflections for MnO and the 330 reflection for Mn. (c) TEM BF image of the layer annealed for 60 min clearly showing the oxide layer. (d) TEM DF image of the annealed zigzag layer in (c) using part of the 111 and 200 reflections for MnO and the 330 reflection for Mn. (e) TEM BF image of the layer annealed for 120 min with the visible oxide layer on the top. (f) TEM DF image of the annealed zigzag layer in (e) using part of the 111 and 200 reflections for MnO and the 330 reflection for Mn. (g) TEM BF image of the layer annealed for 1920 min. (h) TEM DF image of the annealed zigzag layer in (g) using part of the 111 and 200 reflections for MnO and the 330 reflection for Mn. (*Continued*)

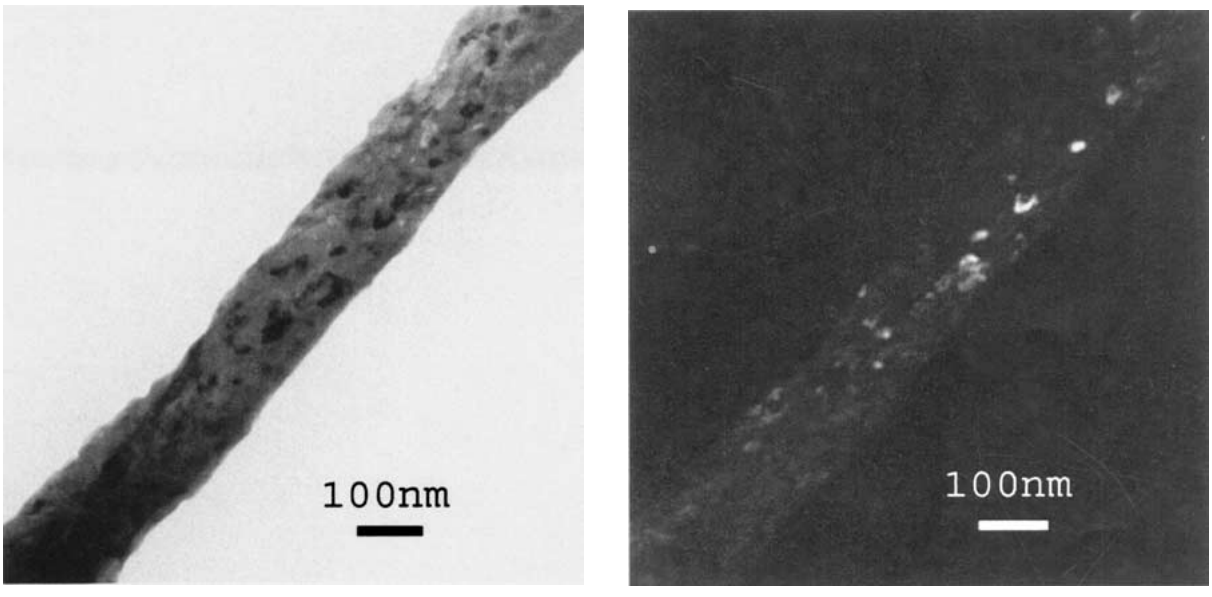

(g) (h)

Figure 8 (*Continued*)

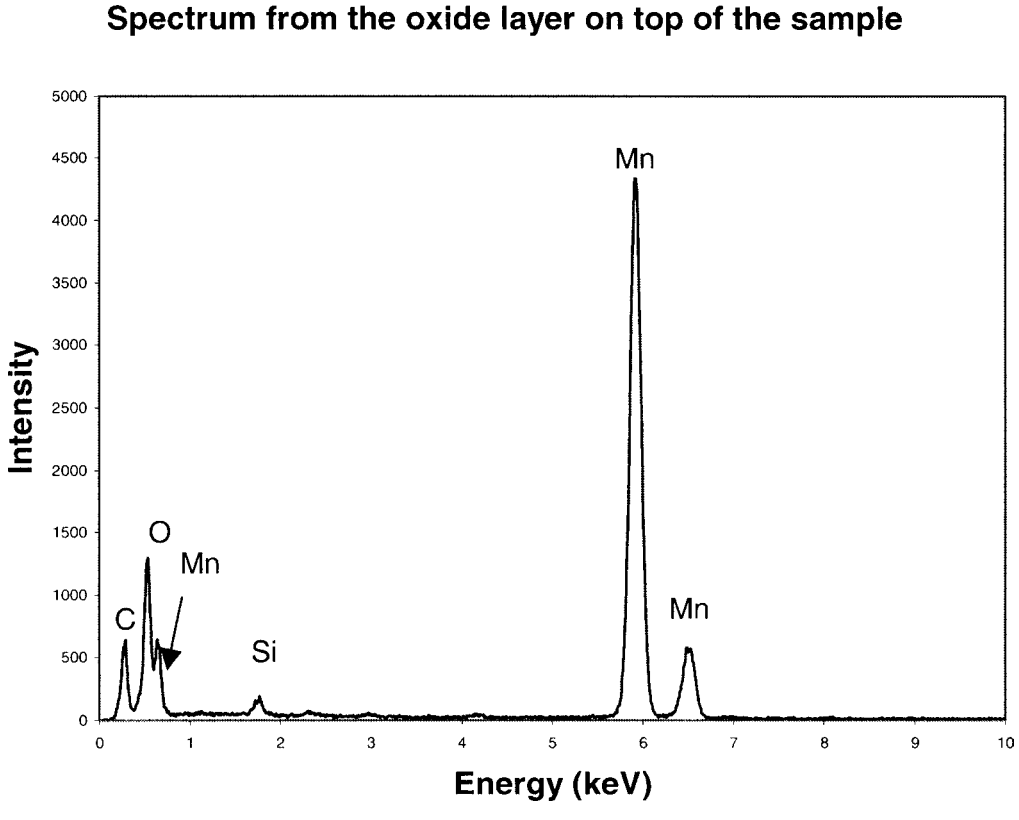

Figure 9 EDX spectrum taken from the oxide layer on top of the manganese zigzag layer that was annealed for 60 min.

not maximized. However, porosity can be increased by increasing the deposition flux angle from 77 to 86° [11].

An energy dispersive X-ray (EDX) spectrum (Fig. 2b), taken from the central region of the zigzag layer indicates that there is oxygen within the manganese zigzag layer. This result suggests that oxidation has occurred during deposition rather than post-deposition. The carbon peak in the spectrum is contamination from the microscope and specimen, while the Si peak is an ion milling artifact from the Si substrate.

Selected area diffraction (SAD) from the zigzag layer resulted in the ring pattern shown in Fig. 2c and corroborates the EDX results. The pattern has been indexed as a mixture of cubic manganese, with a cell parameter of 0.8192 nm, and cubic MnO, with a cell parameter of 0.445 nm.

Although it was expected that only metallic manganese would be deposited, due to the relatively low

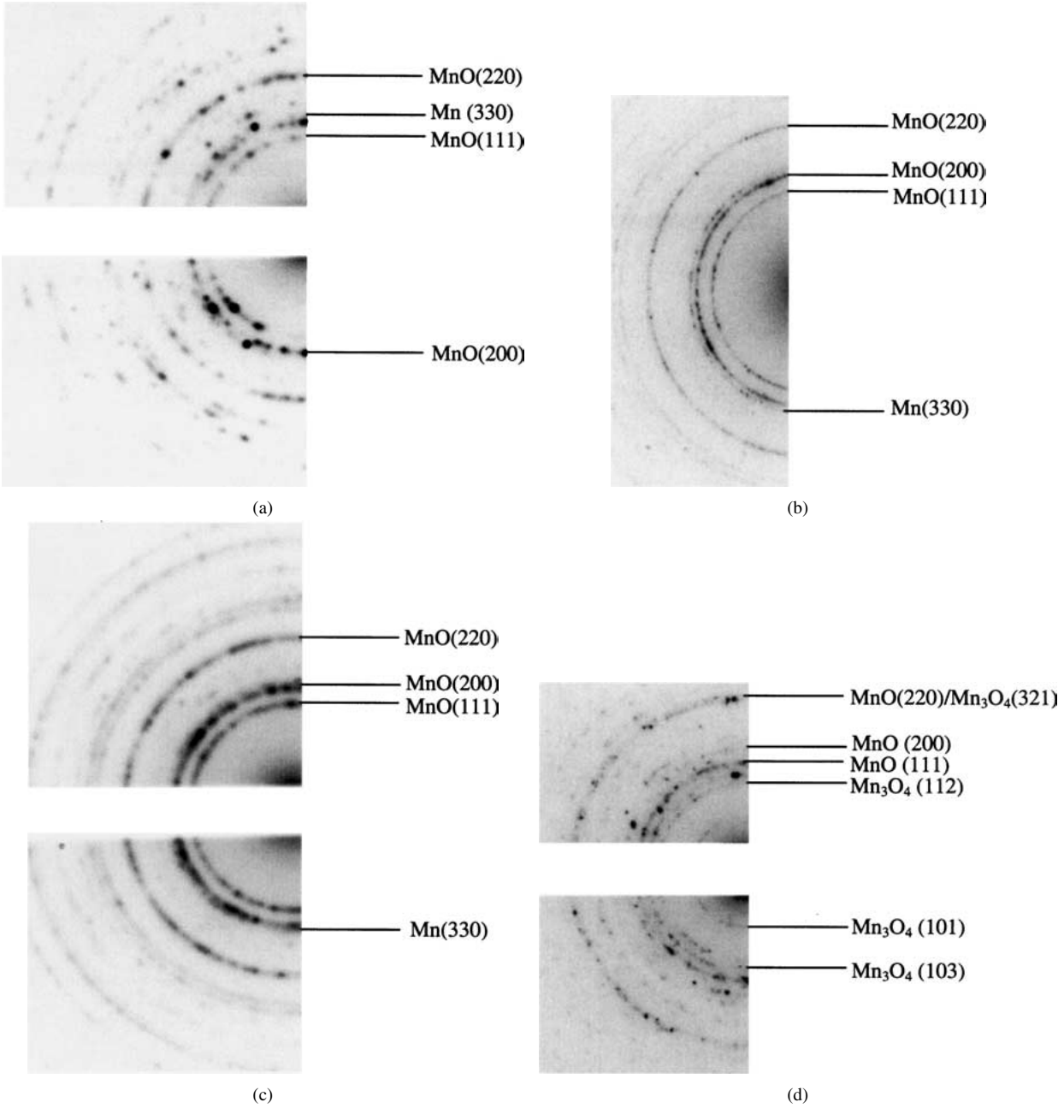

Figure 10 SAD patterns from layer annealed for (a) 30 min, (b) 60 min, (c) 120 min, and (d) 1920 min.

deposition pressure ($\sim 10^{-5}$ torr), it is not unusual for materials to oxidize during a physical vapor deposition process. The SAD pattern was taken from the entire zigzag layer indicating the oxide is present throughout the layer, not just on the surface, suggesting that it formed during the deposition rather than after the deposition. This is also supported by the dark field image of the layer (Fig. 2d), which is formed from part of the 111 and 200 reflections for MnO and the 330 reflection for Mn. Grains ($\sim$20 nm) in size appear throughout the layer. Mn and MnO grains are indistinguishable. The apparent absence of grains from the central portion of the zigzag layer is an artifact of the specimen preparation process. The Mn/MnO layer sputters more slowly than the Pt, Ti or Si, leaving it thicker in the middle.

The X-ray diffraction (Fig. 3) data confirms the EDX and electron diffraction results. The major peaks for both Mn and MnO can be indexed, in addition to the peaks from the Pt layer.

3.2. Electrochemically oxidized sample

Perhaps the most important structure to analyze is the electrochemically-oxidized sample as it is ultimately the material that exhibits the supercapacitive behavior. The as-deposited sample is made active during the first charging cycle by slowly increasing the voltage before the full cycling begins, and it is important to determine what changes are taking place in the material as it becomes active. The structure of the electrochemically oxidized film is shown in Fig. 4 with an accompanying SAD pattern.

It is clear that electrochemical oxidation of the sample occurred without destroying the zigzag structure. This is critical, as the surface area and porous structure

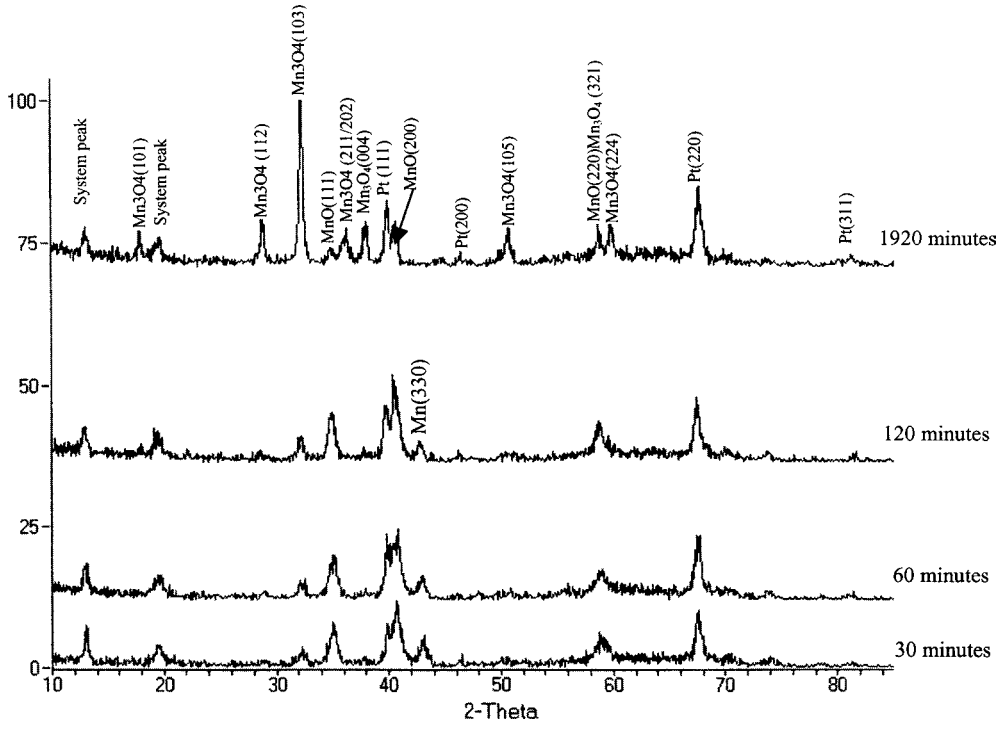

Figure 11 XRD spectra from the four annealed samples indexed to show the disappearance of Mn and the growth of tetragonal Mn_3O_4.

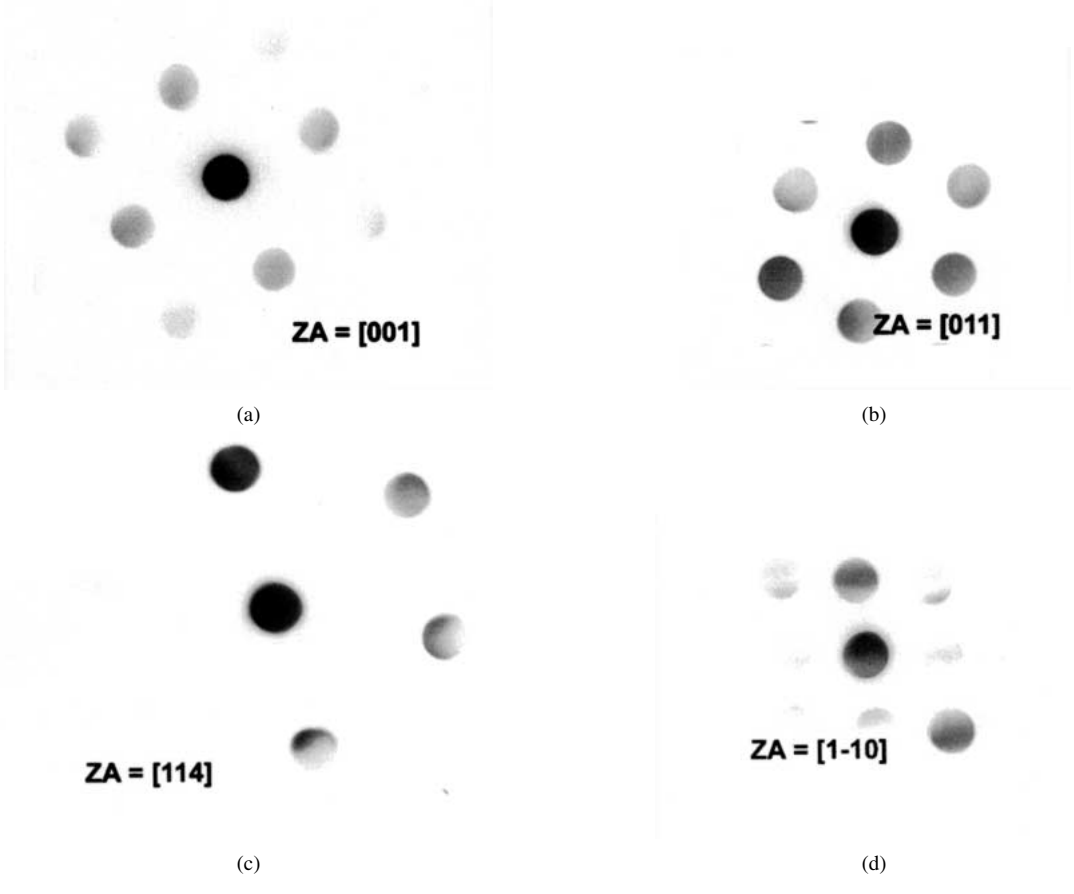

Figure 12 CBED patterns from four different grains in the surface oxide layer. (a), (b) and (c) are indexed as the cubic form of MnO and (d) is indexed as the tetragonal form of Mn_3O_4.

of the original film is preserved. That the structure does not degrade during the capacitive charging and discharging cycle (this particular sample was cycled over 100 times) is an indication that the structure is sufficiently robust for a supercapacitive process. As well, the absence of any noticeable damage suggests that the capacitive reaction is indeed reversible as required. Otherwise, the zigzag structure would likely have experienced some kind of distortion, if an irreversible transition had occurred.

It is clear from the diffraction pattern (Fig. 4c) that a different phase has formed relative to the as-deposited sample. It was indexed to the tetragonal Hausmannite phase (Mn_3O_4). Thus, there is overall oxidation of the initial Mn/MnO structure to Mn_3O_4.

Although an MnO_2 product was expected, based on reports from the literature, Mn_3O_4 is not unheard of and has been recently reported as an electrochemical supercapacitor material [12]. The following redox reactions were proposed in an alkaline medium for electrodeposited Mn_3O_4 [12]. While the first two reactions do not necessarily apply to these films, which are metallic Mn and MnO rather than the pure Mn used by Jiang and Kucernak, the final two reactions may give a good starting point for the possible reversible reactions that occur during the charge/discharge cycle.

$$Mn{\cdot}2H_2O + 2H_2O \Leftrightarrow Mn(OH)_2 + 2H_3O^+ + 2e^-$$

$$3Mn(OH)_2 \Leftrightarrow Mn_3O_4{\cdot}2H_2O + 2H^+ + 2e^-$$

$$Mn_3O_4{\cdot}2H_2O + OH^- \Leftrightarrow MnOOH + Mn(OH)_3 + e^-$$

$$4MnOOH + 2Mn(OH)_3 + OH^- \Leftrightarrow (6MnO_2){\cdot}5H_2O + 3H^+ + 6e^-$$

There are conflicting results in the literature as to whether the capacitance is due to a proton insertion mechanism, or the chemisorption of sodium from the electrolyte. The proposed sodium chemisorption reaction mechanism found in literature is based on an MnO_2 precursor [4]. However, there is no reason to assume that a complementary sodium chemisorption reaction would not occur with the Mn_3O_4 material. For this reason, the sample was viewed at higher magnification in the FEG TEM/STEM. The image is shown in Fig. 5 with corresponding EDX spectra from the each area. A thin surface layer is present on top of the zigzag layer and was found, through EDX analysis to contain much higher levels of Na relative to the bulk material. The effect may simply be due to ordinary absorption mechanisms. Unfortunately, the layer was too thin to be evaluated by convergent beam diffraction. While this result may suggest that a sodium chemisorption mechanism is at work, confirmation is not possible at this time. It is also possible that this surface layer is the result of some irreversibility in the process although this proposition cannot be confirmed by the results.

3.3. Annealed films

In the original work by Broughton, the chevron films were thermally annealed and then electrochemically oxidized in order to determine if any increase in capacitance could be produced. However, the CV scans proved ultimately destructive to the thermally annealed film making useable capacitance measurements impossible [9]. To determine if there was any physical evidence for the poor capacitive performance, the deposited zigzag film was thermally oxidized for 30, 60, 120, and 1920 min and then studied using a combination of SEM and TEM imaging, as well as electron and X-ray diffraction. Fig. 6 shows FE-SEM SE images for the four different annealing times. What becomes immediately obvious from these images is that a columnar layer (identified as an oxide layer by TEM and XRD analysis in subsequent paragraphs) is formed on the top of the zigzag layer. In fact, even at 30 min, the entire zigzag layer is essentially capped. By 1920 min, the bulk of the zigzag layer has been replaced by a porous oxide structure with very little zigzag texture remaining.

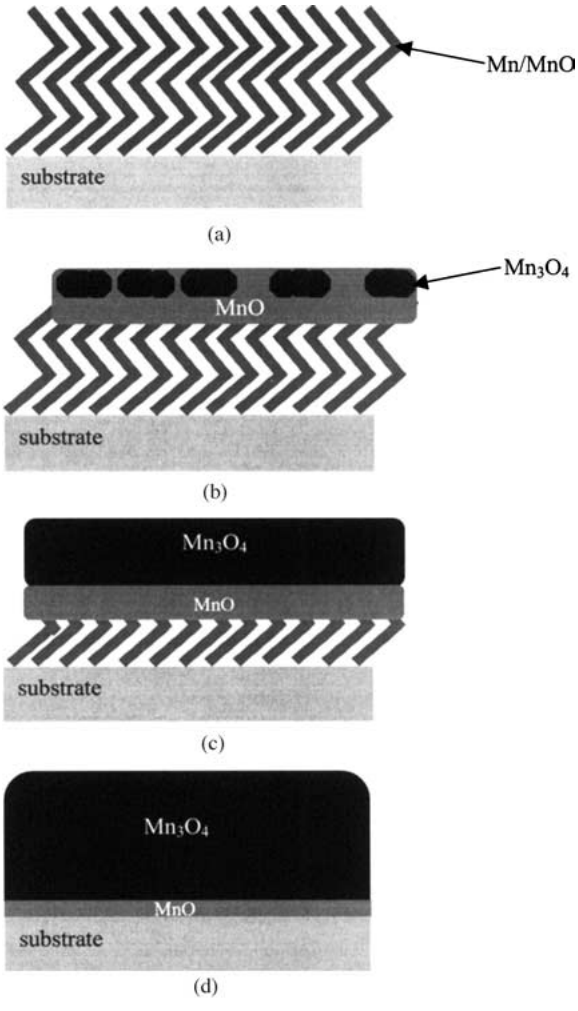

Figure 13 Schematic illustration of oxide growth. (a) The original material composed of Mn and MnO zigzags. (b) and (c) The original zigzag layer slowly transforms to a columnar oxide layer that is both MnO and Mn_3O_4. (d) The final structure in which the original oxide layer has been destroyed and replaced by the columnar oxide layer that is primarily Mn_3O_4 with some MnO.

The formation of this oxide layer on the surface of the zigzags, rather than further oxidation of the material within the zigzag layer itself, may explain the poor capacitance behavior of these films. Once the oxide layer forms, it has significantly reduced the usable surface area and eliminated any porosity, resulting in fewer sites for the redox reaction to occur and therefore a poorer capacitance value.

If the thickness of the oxide film is plotted versus the square root of time (Fig. 7) a linear trend is found. This result implies that oxide growth is diffusion controlled, i.e., $x \propto \sqrt{Dt}$, where x is the thickness of the oxide film, D is the diffusivity and t is the diffusion time. The curve does not pass through $x = 0$ at $t = 0$, which may be accounted for as incubation time for oxide formation.

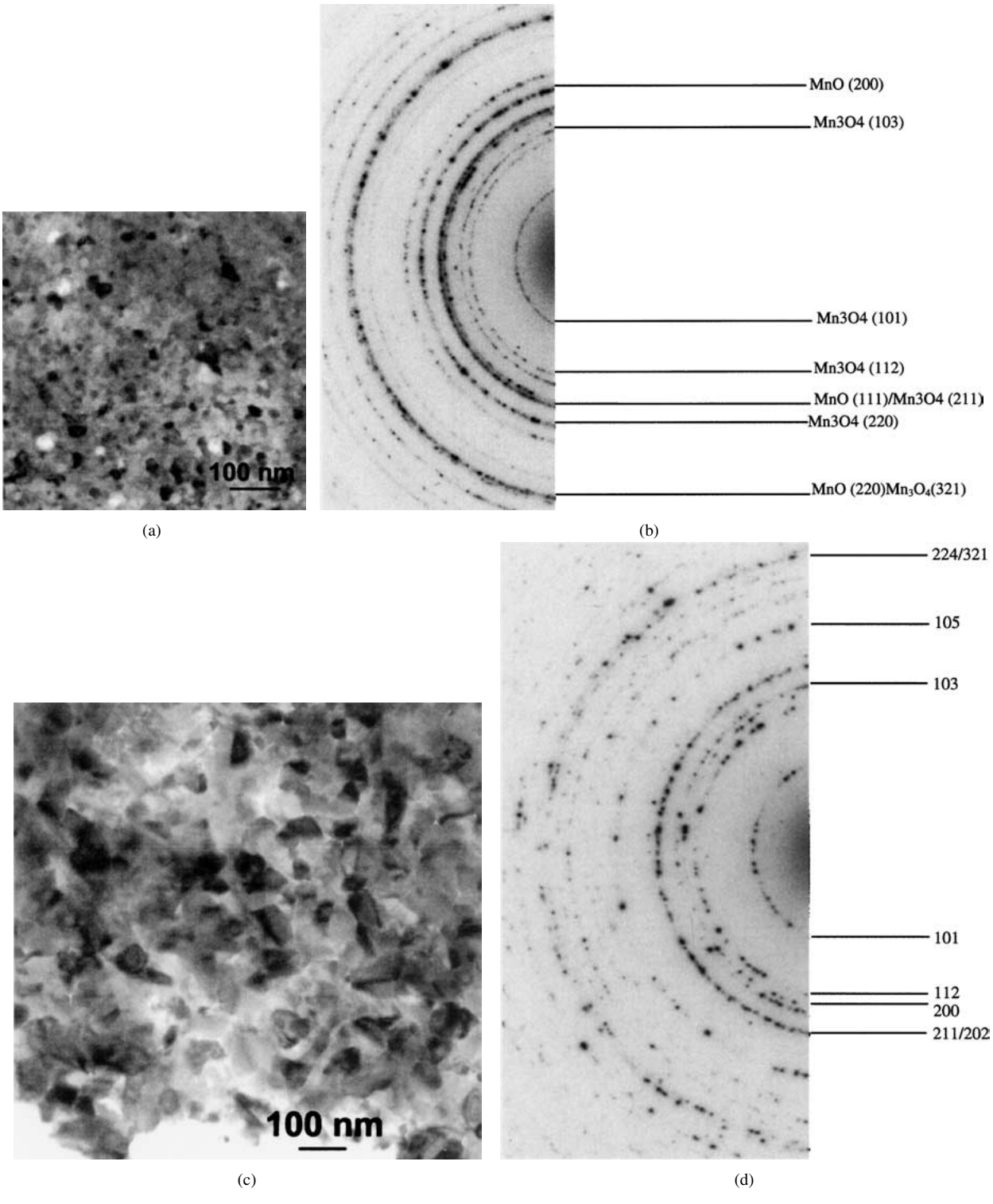

Figure 14 (a) TEM BF image of the plan view section of the sample annealed for 60 min. (b) SAD pattern from the area in the BF image showing the MnO and Mn_3O_4 phases. (c) TEM BF image of the plan view section of the sample annealed for 1920 min. (d) SAD pattern from the area in the BF image showing Mn_3O_4.

The effects of annealing on the internal structure of the zigzag layer were studied using the TEM. Fig. 8 shows both bright field and complementary dark field images of the zigzag layer at the various annealing times. Although the oxide layer is not visible in the sample that was annealed for 30 min (it was sputtered away), it is clearly visible in both the 60 and 120 min samples. EDX spectra taken from the columnar oxide layer in the 60-min sample confirms that it is a manganese oxide (Fig. 9).

Evident in the dark field images is a gradual coarsening of the grains within the zigzag structure from ~25 to ~75 nm. However, it is unlikely that the increase in grain size would result in a decrease in capacitive behavior; it is more likely due to the growth of the oxide capping layer which significantly reduces the useable surface area.

A comparison of the SAD patterns for the four different annealing times is shown in Fig. 10. The first three SAD patterns (Fig. 10a–c) are all indexed as a mixture

of cubic Mn and cubic MnO and are identical to the as-deposited sample. The diffraction pattern in Fig. 10d (1920 min) is different from the others and can be indexed to both MnO and Mn_3O_4. Thus, it appears that the zigzag structure is slowly oxidizing to Mn_3O_4. The XRD spectra for the four annealing conditions (Fig. 11) corroborate the TEM results. The Mn_3O_4 peaks are significantly more intense in the 1920 min sample, relative to the other 3 annealing times. The Mn is consumed during the oxidation process, and is absent in the 1920-min sample. The absence of the Mn_3O_4 rings in the SAD patterns of Fig. 10a–c may just be a sampling phenomenon, as the surface oxide layer makes up only a small portion of the total oxide layer thickness.

Convergent beam electron diffraction (CBED) of individual grains of the oxide was done for further verification of the above analysis. Four CBED patterns, taken from grains in the oxide layer of the 120-min sample, are shown in Fig. 12. CBED was not attempted on the 30 and 60 min samples because the oxide layer was too thin, and the grains too small, to provide suitable patterns. XRD results (Fig. 11) showed that the same oxide was forming on all samples. The first three CBED patterns in Fig. 12a–c are indexed as the cubic form of MnO, while the last CBED pattern (Fig. 12d) is indexed as the tetragonal form of Mn_3O_4, confirming that there are two different oxides in the columnar layer.

Based on the above SEM, TEM and XRD results, the following model is proposed, and illustrated schematically in Fig. 13, for the thermal oxidation process. The as-deposited sample (Fig. 13a) consists of a zigzag structure made up of interspersed grains ($\sim$20 nm in size) of Mn and MnO. As mentioned previously, Mn is oxidized during the physical deposition process. During annealing, the remaining Mn is progressively oxidized to MnO (gray) (Fig. 13b and c). The zigzag morphology is lost during oxidation, due to the volume increase that accompanies MnO formation. The density of MnO (5.43 g/cm^3) is approximately three-quarters of that for Mn (7.20 g/cm^3). As oxidation of Mn proceeds, MnO begins to oxidize to Mn_3O_4 (black), from the surface inwards (Fig. 13b–d). By 1920 min, the original zigzag structure is almost completely consumed, leaving a thick Mn_3O_4 layer covering a thin MnO layer (Fig. 13d). Further annealing would result in complete oxidation to Mn_3O_4.

Further confirmation for the proposed model was obtained through analysis of plan view specimens. Specimen preparation is such that only the outermost layer is visible in the TEM. The image and diffraction pattern, shown in Fig. 14a and b, are from the 60-min sample, which has a fairly thin outer oxide layer ($<$100 nm). The SAD pattern can be indexed as a combination of MnO and Mn_3O_4. However, the sample annealed for 1920 min (Fig. 14c and d) has a diffraction pattern that can be indexed exclusively as Mn_3O_4 confirming the oxidation mechanism proposed in Fig. 13.

This Mn_3O_4 is the same phase that ultimately forms during electrochemical oxidation. However, the fact that the Mn_3O_4 zigzag film that is produced through electrochemical oxidation exhibits supercapacitive qualities while the thermally produced Mn_3O_4 layer, which has a columnar structure, does not, suggests the texture of the film is far more important than the composition.

4. Conclusions

Physical vapor deposition is shown to be a viable method of producing an electrochemical supercapacitor. Although it was intended to deposit the metallic manganese, a mixture of Mn and MnO was actually produced. Furnace annealing the zigzag structure resulted in the growth of a columnar oxide on the surface of the zigzag layer that destroys the original texture of the layer. The growing oxide was found to be the cubic form of MnO and the tetragonal form of Mn_3O_4. These results help explain why the performance of the capacitor decreases upon annealing. The furnace annealing causes the zigzag layer to be capped, resulting in a significant decrease in surface area, that ultimately reduces the capacitance of the film. The form of the oxide that is ultimately used as the supercapacitor is also the tetragonal form of Mn_3O_4. The nature of the re-dox reaction is still speculative, but may involve the surface Na-containing layer that is produced during electrochemical oxidation. Additional work is needed to determine the composition of the film and its role in the capacitive process.

Acknowledgments

The authors would like to acknowledge funding contributions from the Natural Sciences and Engineering Research Council of Canada (NSERC) in addition to the Alberta Informatics Circle of Research Excellence (iCORE).

References

1. B. E. CONWAY, in "Electrochemical Supercapacitors" (Kluwer/Plenum Publishers, NewYork, 1999).
2. R. KOTZ and M. CARLEN, *Electrochimica Acta* **45** (2000) 2438.
3. M. TOUPIN, T. BROUSSE and D. BELANGER, *Chem. Mater.* **14** (2002) 3946.
4. Y. U. JEONG and A. MANTHIRAM, *J. Electrochem. Soc.* **149**(11) (2002) A1419.
5. S. PANG, M. A. ANDERSON and T. W. CHAPMAN, *ibid.* **147**(2) (2000) 444.
6. S. PANG and M. A. ANDERSON, *J. Mater. Res.* **15**(10) (2000) 2096.
7. C. HU and T. TSOU, *Electrochimica Acta* **47** (2002) 3523.
8. H. Y. LEE, S. W. KIM and H. Y. LEE, *Electrochem. Solid-State Lett.* **4**(3) (2001) A19.
9. J. N. BROUGHTON and M. J. BRETT, *ibid.* **5**(12) (2002) A279.
10. S.-F. CHIN, S.-C. PANG and M. A. ANDERSON, *J. Electrochem. Soc.* **149**(4) (2002) A379.
11. K. ROBBIE and M. J. BRETT, *J. Vac. Sci. Technol.* A **15**(3) (1997) 1460.
12. J. JIANG and A. KUCERNAK, *Electrochimica Acta* **47**(15) (2002) 2381.

Received 27 May
and accepted 14 August 2003